Transforming an Insulating Metal—Organic Framework (MOF) into Electrically Conducting
MOF⊃Conducting Polymer Composites

Amina Khatun, Ashok Yadav, Shiyu Zhang, and Sourav Saha\*

Department of Chemistry, Clemson University, Clemson, South Carolina 29634, United States

\*Corresponding Author. Email: souravs@clemson.edu

## **ABSTRACT**

Owing to their diverse potentials to help advance modern electronics and energy technologies, electrically conducting metal-organic frameworks (MOFs) have emerged as one of the most coveted functional materials within the past decade. The key to developing electrically conducting MOFs is to equip them with mobile charge carriers and facilitate long-range charge movement. Circumventing the challenges and unpredictability associated with the construction of intrinsically conducting MOFs, herein, we have converted a structurally robust and porous but intrinsically insulating Zn-dpzNDI MOF based on an electron deficient dipyrazolate-naphthalenediimide (dpzNDI) ligand into electrically conducting MOF conductingpolymer (MOF\(\triangle CP\)) composites via oxidative polymerization of preloaded redox-active 3.4ethylenedioxythiophene (EDOT) and pyrrole (Py) monomers to corresponding PEDOT and PPy polymers, which are well-known hole-transporters. After monomer loading and in-situ polymerization, the resulting MOFDCP composites remained crystalline but became less porous, suggesting that the amorphous CP chains were mostly confined to the MOF cavities. The presence of CPs was confirmed by IR, diffusereflectance UV-Vis-NIR, and STEM-EDX analyses. Whereas the pristine MOF had immeasurably low conductivity ( $\sigma < 10^{-12}$  S/m), the MOF $\supset$ PEDOT and MOF $\supset$ PPy composites displayed significantly higher electrical conductivity:  $1.8 \times 10^{-5}$  and  $2.5 \times 10^{-3}$  S/m, respectively. Thus, we have transformed an intrinsically insulating MOF into electrically conducting MOF CP via in-situ oxidative polymerization of electron-rich monomers, a versatile strategy that could be adopted to engineer this much coveted but elusive electronic property practically in any porous MOFs.

**Keywords:** Metal-organic frameworks, Conducting polymers, MOF-Polymer composites, Electrical conductivity, Oxidative polymerization

#### 1. Introduction

Electrically conducting metal-organic frameworks (MOFs) [1-6], have emerged as one of the most sought functional materials because of their diverse potentials to serve as active components of batteries [7–11], transistors [12,13], supercapacitors [14–16], photovoltaic devices [17–23], chemiresistive sensors [24–30], and electrocatalysts [31-34] and thus help advance electronics and energy technologies. Since electrical conductivity is a product of charge-carrier concentration (i.e., electrons or holes) and mobility, MOFs must possess adequate charge-carriers and efficient long-range charge transport capability to display this much coveted electronic property [2,3]. While redox-active components endow MOFs with requisite chargecarriers, depending on the frameworks' structures and compositions, the charges can flow through either (i) metal-ligand coordination bonds with large covalent character, i.e., high degree of orbital overlap [35– 41], (ii) extended  $\pi$ -conjugated ligands [42–68], (iii) continuous  $\pi$ - $\pi$ - or  $\pi$ -donor/acceptor stacks [69–75], and/or (iv) redox-hopping [76–81]. Intrinsically conducting MOFs possess at least one of these long-range charge transport pathways, however, it is quite challenging to design and synthesize them in a predictable manner because insulating metal-cluster nodes made of ionic coordination bonds and large spatial separation between the ligands—the common features of porous MOFs—hinder through-bond and throughspace charge movement, respectively. An effective way to address these challenges is to exploit MOF's porosity to introduce appropriate guest molecules to facilitate long-range charge movement and thereby boost their electrical conductivity [82–88]. Since most small molecular guests are not intrinsically conducting, the porous MOFs must have certain structural features to help create guest-mediated charge transport pathways, such as coordinatively unsaturated nodes, which can be crosslinked by coordinating  $\pi$ conjugated guests to promote through-bond charge movement [85], or parallel redox-active ligands located at regular intervals that can form extended  $\pi$ -donor/acceptor stacks with intercalated redox-complementary guest π-systems and thereby facilitate through-space charge movement [86–88]. Furthermore, large number of infiltrated guest molecules are often needed to create such long-range charge transport pathways, which diminish the MOF's porosity (although this is not an issue unless the doped materials are intended for electrocatalysis or chemiresistive sensing applications, which require infiltration of substrates and analytes into MOFs).

Building on the versatile guest-induced conductivity approach, recently, electrically conducting polymers (CPs), such as poly-3,4-ethylenedioxythiophene (PEDOT) and polypyrrole (PPy) have been introduced into porous MOFs via monomer infiltration, followed by *in-situ* oxidative polymerization, which yielded MOF¬CP composites with significantly improved conductivity [89–96]. In biporous MOFs having two distinct cavities, such as MIL-101(Cr), MIL-100(Fe), and UiO-66, the CPs formed predominantly inside the larger pores while the smaller pores remained mostly empty, thus partly preserving the MOFs'

porosity while significantly boosting their conductivity. Since the embedded CPs acted as charge-carrier sources as well as charge transporters, in principle, this strategy could be adopted to boost the electrical conductivity of any porous MOFs. Expanding the scope of this elegant strategy, herein, we demonstrate that an insulating porous Zn-dpzNDI MOF (dpzND dipyrazolate-naphthalenediimide (dpzNDI) ligand having uniform pores and channels [97], can also be converted to electrically conducting MOF $\supset$ CP composites by first loading it with EDOT and pyrrole, followed by oxidative polymerization of pre-loaded monomers into corresponding PEDOT and PPy polymers (Scheme 1). The resulting MOF $\supset$ CP composites remained highly crystalline, although their surface areas diminished significantly due to the formation of CP chains inside the MOF pores. The in-situ formation of PEDOT and PPy polymers was confirmed by IR and UV-Vis-NIR diffuse reflectance spectroscopies (DRS), MALDI-ToF mass spectrometry, and STEM-EDX analysis. Whereas the pristine MOF is an electrical insulator ( $\sigma \leq 10^{-12}$  S/m) [79], the resulting MOF $\supset$ PEDOT and MOF $\supset$ PPy composites displayed up to billion times higher conductivity ( $\sigma \sim 10^{-5}$  and  $10^{-3}$  S/m, respectively), demonstrating that practically any porous MOFs that can allow appropriate monomer infiltration, followed by oxidative polymerization, can be used to develop electrically conducting MOF $\supset$ CP composites through this strategy.

**Scheme 1.** The preparation of MOF⊃CP composites.



# 2. Materials and Experimental Section

Synthesis of Zn-dpzNDI MOF. All chemicals were used as received. The dpzNDI ligand and Zn-dpzNDI MOF were synthesized according to reported protocols [97]. Briefly, a mixture of 1,4,5,8-naphthalene tetracarboxylic dianhydride (300 mg, 1.12 mmol) and 3,5-dimethyl-1H-pyrazol-4-amine (274.29 mg, 2.382 mmol) was refluxed in anhydrous DMF (15 mL) under N<sub>2</sub> atmosphere for 8 h. Upon adding Et<sub>2</sub>O to the

dark brown reaction mixture, a yellowish orange solid precipitated out, which was filtered and recrystallized from DMF/Et<sub>2</sub>O mixture to obtain dpzNDI ligand. The NMR of the product matched well with the reported one. To synthesize the MOF, dpzNDI ligand (40 mg, 0.088 mmol) and  $Zn(NO_3)_2.6H_2O$  (28.4 mg, 0.096 mmol) were dissolved in DMF (7 mL) in a screw-capped vial and kept in a 130 °C oven for 24 h. The orange-colored MOF was washed thoroughly with DMF, MeOH, and Et<sub>2</sub>O, and activated at 120 °C under vacuum for 24 h.

Synthesis of MOF ¬PEDOT composite. The activated pristine MOF (100 mg) was soaked in EDOT (10 μL) / Et<sub>2</sub>O solution (15 mL) for 48 h. After removing the solvent and excess monomers under reduced pressure, the resulting EDOT-loaded MOF was treated with iodine vapor at 90 °C for 48 h to polymerize the infiltrated monomers into PEDOT, according to a literature protocol [91,92]. The resulting black solid was washed consecutively with hexane, methanol, water, and acetone to remove excess iodine and dried overnight under vacuum to obtain MOF¬PEDOT.

Synthesis of MOF⊃PPy composite. Following a slightly modified reported protocol [92,98], the activated pristine MOF (75 mg) was soaked in pyrrole (1.5 mL) under N₂ for 48 h., then excess pyrrole was removed under reduced pressure, the monomer-loaded MOF was treated with iodine / hexane solution (0.05 M) at room temperature for 24 h, then the resulting material was washed with hexane, methanol, and acetone, and drying under vacuum to obtain MOF⊃PPy composite a black powder.

Synthesis of Bulk PEDOT. Bulk PEDOT was synthesized by heating a solution mixture of EDOT (0.25 g, 1.75 mmol) and iodine (1.12g, 4.4 mmol) in toluene (15 mL) at 90 °C for 48 h, followed by washing the resulting black mass thoroughly with hexane and acetone [91,92].

Synthesis of Bulk PPy. Bulk PPy was synthesized by adding an aqueous  $FeCl_3$  solution slowly to pyrrole (molar ratio of  $FeCl_3$ : Py = 2.3 : 1) and stirring the resulting solution at room temperature for 24 h. followed by washing the resulting black solid with water and methanol. [99].

 $I_2$ -treated MOF. The activated pristine MOF was treated with iodine vapor at 90 °C for 48 h. and the resulting material was then washed with hexane, methanol, water, and acetone dried overnight under vacuum to remove excess iodine. This material was used as a control.

*Extraction of CPs.* The MOF⊃CP composites were immersed in an aqueous NaOH solution for 48 h which digested the coordination framework. The residual black polymeric mass was washed with water and methanol to obtain extracted PEDOT and PPy [91]. Based on the weight of extracted CP from respective MOF⊃CP composite, MOF⊃PEDOT contained 33 wt% PEDOT and MOF⊃PPy contained 18 wt% PPy.

Characterization methods. The  $^1$ H NMR spectra were recorded on a Bruker 500 MHz NMR spectrometer, MALDI-ToF mass spectra on a Bruker Autoflex instrument, and powder X-ray diffraction (PXRD) patterns on a Rigaku Ultima IV X-ray diffractometer equipped with Cu K $\alpha$  radiation source ( $\lambda$  = 1.5406 Å) and a CCD area detector. The UV-Vis-NIR DRS plots were recorded with a Shimadzu UV-2600 spectrophotometer equipped with an integrated sphere and FT-IR spectra with a Thermo-Nicolet Nexus 670 FT-IR/NIR Spectrometer. Thermogravimetric analysis was conducted on an SDT Q600 instrument. The surface area was determined from  $N_2$  sorption isotherms measured with a Quantachrome Autosorb iQ Gas Sorption Analyzer. STEM-EDX analyses were performed with a Hitachi SU-9000 SEM/STEM instrument with EDX capability.

Electrical conductivity measurements. The electrical conductivity of these materials was determined from current-voltage (I-V) measurements under ambient conditions (293 K) using in-situ pressed pellets of each material [68,74,75]. A two-probe device consisting of two precision-cut stainless-steel rods with flat round tips (radius = 0.135 cm) partially inserted into a snugly fit Teflon tube securing the pellet sandwiched between the two steel rods was used for two-probe electrical measurements. The tips of the steel rods were precoated with silver paint for better electrical contact between the electrodes and sandwiched MOF materials. Each pellet was prepared from 2.5 mg of respective material placed between the two silver-coated steel rods inserted in a Teflon tube and then pressed under a constant 260 MPa pressure for 1 min using a digital Parr pellet press. The thickness (L  $\approx$  0.02 cm) of MOF pellets was measured from the difference in the total length of two steel rods with and without the sandwiched materials using a digital caliper, and the area ( $A = 0.057 \text{ cm}^2$ ) was defined by the radius of the steel rods inserted inside the Teflon tube. The corresponding conductivities were calculated using the equation:  $\sigma = L/RA$  (R = total resistance of the pellet obtained from the slope of the corresponding I-V plots). For temperature-dependent I-V measurements, the same setup was immersed in a temperature-controlled sand bath, and the temperature was measured precisely by a pair of digital thermocouples. The devices were held at each temperature for 30 min before measuring their I-V plots to ensure the accuracy of the measurements. The activation energy  $(E_{\rm a})$  was calculated from the temperature-dependent conductivity data using the Arrhenius equation:  $\sigma = Aexp(\frac{Ea}{pT})$ where A = a pre-exponential factor, R = gas constant, and T = temperature in Kelvin.

### 3. Results and Discussions

To explore the versatility of MOF⊃CP composite strategy to boost the electrical conductivity of porous MOFs, herein, we have employed a highly porous Zn-dpzNDI MOF (Fig. 1) based on an electron deficient dpzNDI ligand, which has uniform pores and open channels. We have chosen this MOF for this purpose because (i) the activated material reportedly has a permanent porosity and fairly large surface area [97],

which should allow infiltration of monomers and oxidizing agents and in-situ polymerization, and (ii) the  $\pi$ -acidic NDI ligands are resistant to oxidation, which should allow selective oxidation of infiltrated monomers into CPs and leave the host framework unaffected, allowing us to delineate the effect of embedded CPs on the conductivity of the resulting composites. Zn-dpzNDI MOF was obtained as a crystalline orange powder via a solvothermal reaction between Zn(NO<sub>3</sub>)<sub>2</sub> and dpzNDI in DMF at 130 °C according to a literature protocol [97]. The powder x-ray diffraction (PXRD) pattern of evacuated MOF matched well with the reported pattern (Fig. 1). The activated MOF possessed a large Brunauer-Emmett-Teller (BET) surface area of the activated MOF (1523 m²/g), which was measured from its N<sub>2</sub>-sortption isotherms at 77 K (Fig. S1), indicating that it was suitable for monomer loading and subsequent oxidative polymerization.

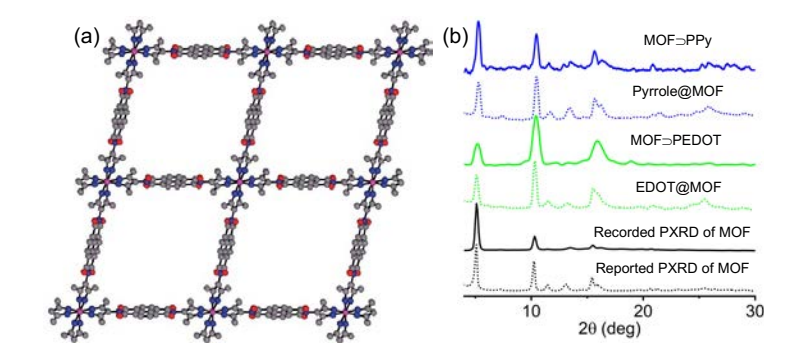


**Fig. 1.** (a) The simulated structure of MOF. grey: C, red: O, blue: N, pink: Zn (adopted from ref. 97 with copyright permission from Royal Society of Chemistry 2013). (b) The PXRD patterns of pristine MOF (dotted black: reported, solid black: recorded), EDOT-loaded MOF (dotted green), MOF⊃PEDOT (solid green), pyrrole-loaded MOF (dotted blue), MOF⊃PPy (solid blue).

To determine the effect of two different CPs (i.e., PEDOT and PPy) on the conductivity of corresponding MOF⊃CP composites, we have introduced electron rich EDOT and pyrrole monomer and oxidatively polymerized the infiltrated monomers into CPs inside the MOF (Scheme 1). To prepare MOF⊃PEDOT composite, the activated MOF was first soaked in an EDOT / Et<sub>2</sub>O solution for 48 h. After removing excess monomer and solvent molecules under reduced pressure, the EDOT-loaded MOF was treated with I<sub>2</sub> vapor at 90 °C for 48 h to generate PEDOT, which turned the orange MOF powder into black. The resulting black powder was washed extensively with hexane, methanol, water, and acetone and dried under vacuum to obtain MOF⊃PEDOT composite. Likewise, the activated MOF was soaked in pyrrole under N<sub>2</sub> for 48 h, the excess pyrrole was removed under reduced pressure, the pyrrole-loaded MOF was treated with an iodine/hexane solution at room temperature, and the resulting black solid was washed thoroughly with hexane, methanol, and acetone to obtain the MOF⊃PPy composite. The PXRD profiles of

that the in-situ generated CPs did not affect the MOF's structure and crystallinity, nor did they only coat the outer surfaces of MOF crystallites, which would have significantly diminished the crystallinity of the MOF. Thermogravimetric analysis revealed that (Fig. S2) the pristine MOF and both MOF $\supset$ CP composites were thermally stable up to at least 300 °C, whereas free PEDOT and PPy started to decompose above 100 °C, demonstrating that the MOF helped stabilize embedded CPs—a notable benefit of encapsulating these CPs inside the MOF.

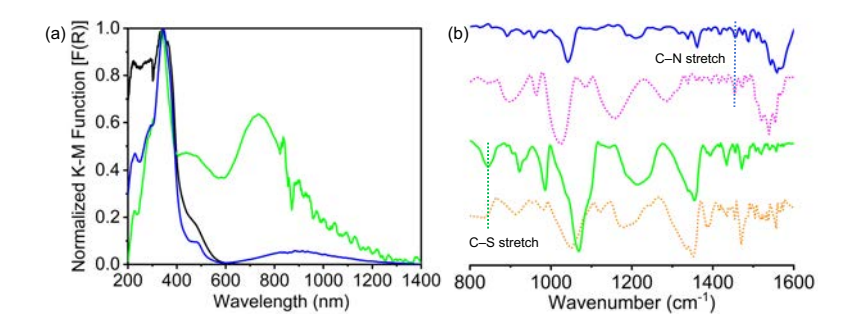


**Fig. 2.** (a) UV-Vis-NIR DRS of MOF (black), MOF⊃PEDOT (green) and MOF⊃PPy (blue) and (b) FT-IR spectra of bulk PEDOT (dotted orange), extracted PEDOT (solid green), bulk PPy (dotted pink), and extracted PPy (solid blue).

The UV-Vis-NIR DRS (Fig. 2a) of orange-colored pristine MOF displayed a characteristic dpzNDI absorption peak at ~375 nm with a shoulder at ~475 nm, whereas black MOF⊃PEDOT and MOF⊃PPy powders displayed prominent NIR peaks centered on ca. 900 and 750 nm, respectively (in addition to the MOF peak), which corresponded to the embedded CP's absorption. To further characterize the embedded CPs, MOF⊃CP composites were treated with aqueous NaOH solution to digest the framework and release the CPs as black solids. The FT-IR spectra (Fig. 2b) of residual CPs extracted from the digested composites were in good agreement with that of pure CPs. For example, separately synthesized pure PEDOT and the MOF-extracted PEDOT both displayed characteristic IR stretching frequencies of C–S (840 cm<sup>-1</sup>), C–O (1070 and 1210 cm<sup>-1</sup>), C–C (1350 cm<sup>-1</sup>), and C=C (1520 cm<sup>-1</sup>) bonds [100]. Likewise, the pure and extracted PPy displayed (Fig. 2b) characteristic IR stretching frequencies of C–N (1450 cm<sup>-1</sup>) and C=C (1520 cm<sup>-1</sup>) bonds [101]. Furthermore, MALDI-TOF analysis (Fig. S3) of extracted PEDOT revealed characteristic m/z peaks of 4–7-mers, whereas the MS data of extracted PPy displayed m/z peaks corresponding to 7–16-mers, suggesting that the degree of in-situ polymerization and average chain length of the latter was greater for PPy than PEDOT.

Compared to pristine MOF, which has a large BET surface area (1528 m<sup>2</sup>/g), MOF $\supset$ PEDOT and MOF $\supset$ PPy composites displayed much smaller surfaces areas (28 and 283 m<sup>2</sup>/g, respectively, Fig. S1), as the in-situ generated CPs occupied the channels. The larger surface area of MOF $\supset$ PPy than MOF $\supset$ PEDOT could be attributed to the following factors: Since the average chain length of extracted PPy (n = 7–16) was longer than extracted PEDOT (n = 4–7), it is plausible that fewer PPy strands were formed than shorter and thicker PEDOT strands (EDOT is a larger molecule than pyrrole), and the latter filled more space inside the MOF channels, making MOF $\supset$ PEDOT less porous.

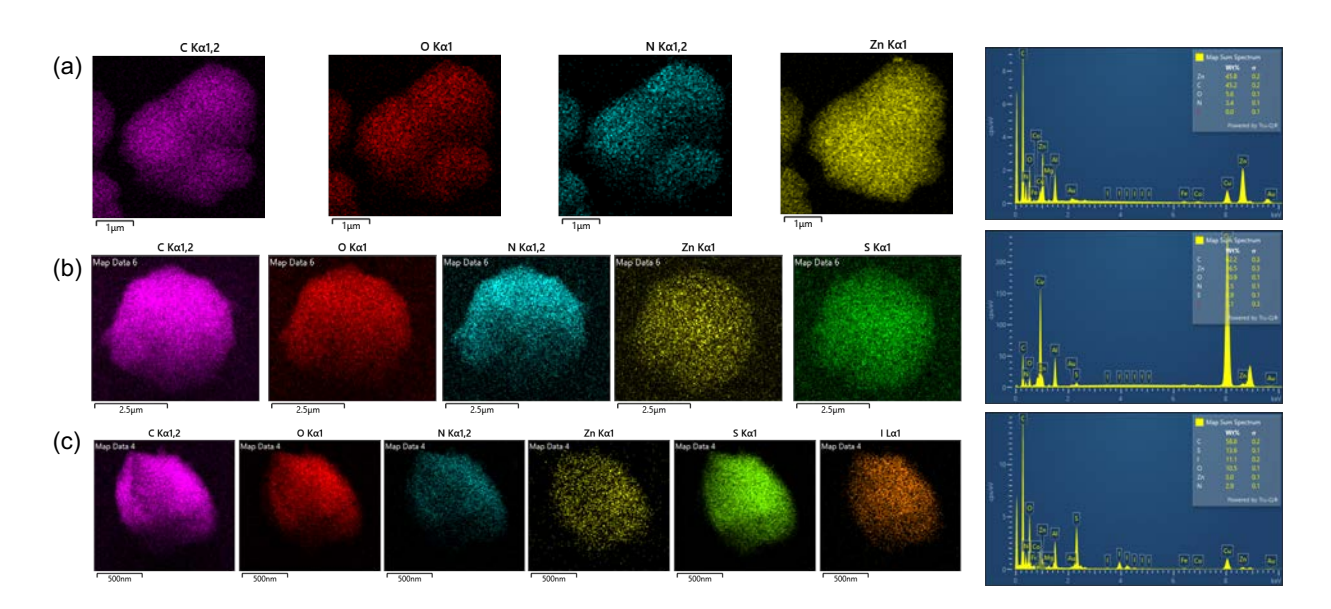


**Fig. 3.** STEM-EDX elemental mapping images of (a) pristine MOF, (b) MOF⊃EDOT, and (c) MOF⊃PEDOT showing coexistence of characteristic elements in the composite. C: pink, O: red, N: cyan, Zn: yellow, S: green, and I: orange.

The microscopic shapes and atomic compositions of pristine MOF, MOF⊃EDOT, and MOF⊃PEDOT were further investigated by STEM-EDX analysis (Fig. 3), which revealed the coexistence of characteristic elements of MOF (Zn and N) and PEDOT (S and I) only in the composite. The coexistence and uniform distributions of Zn, N, S, and I throughout the MOF⊃PEDOT further indicated a uniform presence of PEDOT inside the MOF. The presence of the I-peak in thoroughly washed and vacuum-dried MOF⊃PEDOT sample suggested that the PEDOT chains were partially oxidized and accompanied by charge balancing I⁻ counterions. A similar analysis was not useful for MOF⊃PPy because both MOF and PPy contained C and N, however, a similar scenario is also expected in this case, as all other studies indicated the presence of PPy.

Finally, room temperature electrical conductivities of the MOF, MOFDCP composites, and free bulk CPs were determined from current-voltage (I-V) plots (Fig. 4) measured by two-probe method using pressed pellets of respective materials sandwiched between two stainless steel electrodes surrounded by a snugly fit Teflon tube [68,74,75]. Whereas pristine and iodine-treated MOFs displayed (Fig. 4 and S4) negligible conductivity ( $< 10^{-12}$  S/m), indicating that iodine treatment in the absence of any monomer did not enhance the MOF's conductivity, MOF¬PEDOT and MOF¬PPy composites displayed much higher electrical conductivity ( $1.8 \times 10^{-5}$  and  $2.5 \times 10^{-3}$  S/m, respectively), with the latter showing over a billionfold improvement from the insulating pristine MOF. In contrast, free CPs prepared separately and those extracted from respective MOF CP composite displayed (Fig. 4 and S4) noticeably lower conductivity (PEDOT:  $1.9 \times 10^{-6}$  S/m (bulk),  $1.3 \times 10^{-8}$  S/m (extracted); PPy:  $1.2 \times 10^{-3}$  S/m (bulk),  $1.4 \times 10^{-5}$  S/m (extracted)). The higher intrinsic electrical conductivity of PPy than PEDOT was reflected in the conductivities of MOFDCP composites, suggesting that the CPs were primarily responsible for the conductivity of these composites since the MOF was practically insulating. Furthermore, the conductivity of each in-situ generated MOF CP composite was also significantly higher than that of the mixtures of pristine MOF and separately prepared bulk CPs blended in the same wt/wt ratios as those found in respective MOF⊃CP composite: MOF/33 wt% PEDOT blend: 8.1 × 10<sup>-8</sup> S/m, MOF/18 wt% PPy blend:  $4.2 \times 10^{-5}$  S/m (Fig. S4). The noticeably higher conductivity of each MOF $\supset$ CP composite than the respective MOF/CP blend demonstrated that the composites' conductivities are not just the summation or average of two materials (MOF and CP) conductivities. Together, these results demonstrated the benefits of MOF⊃CP composites prepared by in-situ polymerization over free CPs and MOF/CP blends.

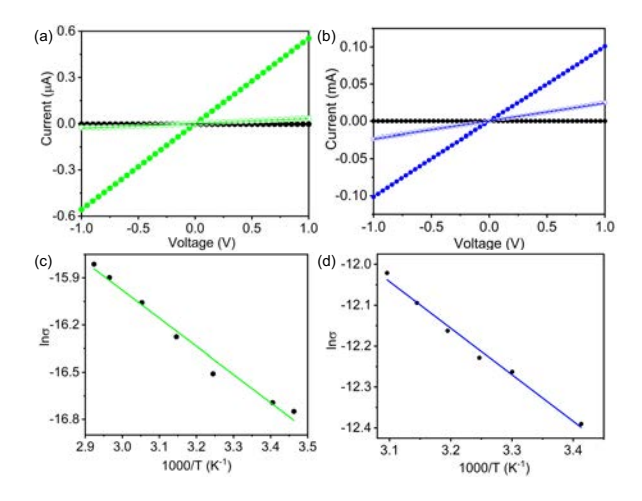


**Fig. 4.** (a, b) The *I-V* plots of pristine MOF (black), MOF⊃PEDOT (solid green circles), bulk PEDOT (open green circles), MOF⊃PPy (solid blue circles), and bulk PPy (open blue circles). (c, d) Arrhenius plots of temperature dependent conductivity values of MOF⊃PEDOT (green) and MOF⊃PPy (blue).

#### 4. Conclusion

The foregoing studies demonstrated that the electrical conductivity of practically any porous MOFs, including those with continuous open channels, can be enhanced significantly via in-situ polymerization of preloaded monomers into electrically conducting polymers, which not only supply mobile charge carriers but also facilitate long-range charge movement. The highly ordered structure of the MOF helped organize the embedded CPs in such a way that the MOF¬CP composites exhibited even higher conductivity than pure CPs, and the conductivities of the composites were much greater than the summation of intrinsic conductivities of two materials, demonstrating the benefit of combining them through this elegant strategy. The conductivities of MOF¬CP composites and free CPs followed the same trend (PPy > PEDOT), demonstrating that the embedded CPs were indeed responsible for the conductivity of these composites. Thus, this work demonstrated the versatility of CP@MOF strategy to convert electrically insulating porous MOFs into conducting MOF¬CP composites. The ability to combine these two dueling properties through this strategy could potentially expand the utility of electrically conducting MOF¬CP composites in chemiresistive sensing and electrocatalysis [102–105].

# Data availability

The raw data is not available for sharing because these data are also used for ongoing studies. The processed data presented in the manuscript can be requested for reproduction and presentation purposes.

#### **Author credit statement**

Amina Khatun, Ashok Yadav, and Shiyu Zhang: synthesis, experiments, data acquisition and analysis, manuscript draft writing, reviewing and editing.

Sourav Saha\*: conceptualization, supervision, data interpretation, manuscript writing, reviewing, and editing.

### **Declaration of competing interest**

Authors declare that no competing financial or personal interest.

## Acknowledgements

This work was supported by the US National Science Foundation (award no. NSF-1809092).

# Appendix A. Supplementary data

Supplementary data of this article can be found online at https://doi.

### References

- [1] M. Jacoby, Conductive MOFs: Surprising charge transport property could lead to new applications, *C&EN* **2021**, *99* (43), 30–34. https://doi/10.1021/cen-09943-cover
- [2] L. Sun, M. G. Campbell, M. Dincă, Electrically Conductive Porous Metal–Organic Frameworks. Angew. Chem. Int. Ed. 55 (2016) 3566–3579. <a href="https://doi.org/10.1002/anie.201506219">10.1002/anie.201506219</a>
- [3] L. S. Xie, G. Skorupskii, M. Dincă, Electrically Conductive Metal–Organic Frameworks. Chem. Rev. 120 (2020) 8536–8580. 10.1021/acs.chemrev.9b00766.
- [4] M. Ko, L. Mendecki, K. A. Mirica, Conductive Two-Dimensional Metal–Organic Frameworks as Multifunctional Materials, Chem. Commun. 54 (2018) 7873–7891. 10.1039/C8CC02871K.
- [5] M. A. Gordillo, S. Saha, Strategies to Improve Electrical and Ionic Conductivities of Metal–Organic Frameworks, Comments on Inorg. Chem. 40 (2020) 86–106. 10.1080/02603594.2019.1704738.
- [6] E. Johnson, S. Ilic, A. J. Morris, Design Strategies for Enhanced Conductivity in Metal-Organic Frameworks, ACS Cent. Sci. 7 (2021) 445–453. 10.1021/acscentsci.1c00047.
- [7] S. S. Park, Y. Tulchinsky, M. Dincă, Single-ion Li<sup>+</sup>, Na<sup>+</sup>, and Mg<sup>2+</sup> Solid Electrolytes Supported by a Mesoporous Anionic Cu–Azolate Metal–Organic Framework, J. Am. Chem. Soc. 139 (2017) 13260–13263. 10.1021/jacs.7b06197.
- [8] D. K. Panda, K. Maity, A. Palukoshka, F. Ibrahim, S. Saha, Li<sup>+</sup> Ion Conducting Sulfonate-Based Neutral Metal–Organic Framework, ACS Sus. Chem. Eng. 7 (2019) 4619–4624. 10.1021/acssuschemeng.8b06254.
- [9] H. Jiang, X.-C. Liu, Y. Wu, Y. Shu, X. Gong, F.-S. Ke, H. Deng, Metal-Organic Frameworks for High Charge-Discharge Rates in Lithium-Sulfur Batteries, Angew. Chem. Int. Ed. 57 (2018) 3916–3921. doi: 10.1002/anie.201712872.
- [10] S. S. Shinde, C. H. Lee, J.-Y. Jung, N. K. Wagh, S.-H. Kim, D.-H. Kim, C. Lin, S. U. Lee, J.-H. Lee, Unveiling Dual-Linkage 3D Hexaiminobenzene Metal-Organic Frameworks towards Long-Lasting Advanced Reversible Zn-Air Batteries, Energy Environ. Sci. 12 (2019) 727–738. 10.1039/C8EE02679C.
- [11] K. W. Nam, S. S. Park, R. dos Reis, V. P. Dravid, H. Kim, C. A. Mirkin, J. F. Stoddart, Conductive 2D Metal-Organic Framework for High-Performance Cathodes in Aqueous Rechargeable Zinc Batteries, Nat. Commun. 10 (2019) 4948. 10.1038/s41467-019-12857-4.
- [12] G. Wu, J. Huang, Y. Zang, J. He, G. Xu, Porous Field-Effect Transistors Based on a Semiconductive Metal-Organic Framework, J. Am. Chem. Soc. 139 (2017) 1360–1363. 10.1021/jacs.6b08511.
- [13] B. Wang, Y. Luo, B. Liu, G. Duan, Field-Effect Transistor Based on an in Situ Grown Metal-Organic Framework Film as a Liquid-Gated Sensing Device, ACS Appl. Mater. Interfaces 119 (2019) 35935-35940. 10.1021/acsami.9b14319.
- [14] D. Sheberla, J. C. Bachman, J. S. Elias, C.-J. Sun, Y. Shao-Horn, M. Dincă, Conductive MOF Electrodes for Stable Supercapacitors with High Areal Capacitance, Nat. Mater. 16 (2017) 220–224. 10.1038/nmat4766.
- [15] W.-H. Li, K. Ding, H.-R. Tian, M.-S. Yao, B. Nath, W.-H. Deng, Y. Wang, G. Xu, Conductive Metal-Organic Framework Nanowire Array Electrodes for High-Performance Solid-State Supercapacitors, Adv. Funct. Mater. 27 (2017) 1702067. <a href="https://doi.org/10.1002/adfm.201702067">10.1002/adfm.201702067</a>.
- [16] H. Wu, W. Zhang, S. Kandambeth, O. Shekhah, M. Eddaoudi, H. N. Alshareef, Conductive Metal-Organic Frameworks Selectively Grown on Laser-Scribed Graphene for Electrochemical Microsupercapacitors, Adv. Energy Mater. 9 (2019) 1900482. 10.1002/aenm.201900482.
- [17] M. E. Foster, J. D. Azoulay, B. M. Wong, M. E. Allendorf, Novel Metal–Organic Framework Linkers for Light Harvesting Applications, Chem. Sci. 5 (2014) 2081–2090. <u>10.1039/C4SC00333K</u>.

- [18] W. A. Maza, A. J. Haring, S. R. Ahrenholtz, C. C. Epley, S. Y. Lin, A. J. Morris, Ruthenium (II)-Polypyridyl Zirconium (IV) Metal–Organic Frameworks as a New Class of Sensitized Solar Cells, Chem. Sci. 7 (2016) 719–727. 10.1039/C5SC01565K.
- [19] J. Liu, W. Zhou, J. Liu, Y. Fujimori, T. Higashino, H. Imahori, X. Jiang, J. Zhao, T. Sakurai, Y. Hattaori, W. Matsuda, S. Seki, S. K. Garlapati, S. Dasgupta, E. Redel, L. Sun, C. Wöll, A New Class of Epitaxial Porphyrin Metal–Organic Framework Thin-Films with Extremely High Photocarrier Generation Efficiency: Promising Materials for All Solid-State Solar Cells, J. Mater. Chem. A 4 (2016) 12739–12747. DOI 10.1039/C6TA04898F.
- [20] H. J. Park, M. C. So, D. Gosztola, G. P. Wiederrecht, J. D. Emery, A. B. F. Martinson, S. Er, C. E. Wilmer, N. A. Vermeule, A. Aspuru-Guzik, J. F. Stoddart, O. K. Farha, J. T. Hupp, Layer-by-Layer Assembled Films of Perylene Diimide- and Squarene-Containing Metal-Organic Framework-Like Materials: Solar Energy Capture and Directional Energy Transfer, ACS Appl. Mater. Interfaces 8(2016) 24983–24988. 10.1021/acsami.6b03307.
- [21] R. Kaur, K-H. Kim, A. K. Paul, A. Deep, Recent Advances in the Photovoltaic Applications of Coordination polymers and Metal Organic Frameworks, J. Mater. Chem. A (4) 2016 3991–4002. 10.1039/C5TA09668E.
- [22] E. D. Spoerke, L. J. Small, M. E. Foster, J. Wheeler, A. M. Ullman, V. Stavila, M. Rodriguez, M. D. Allendorf, MOF-Sensitized Solar Cells Enabled by a Pillared Porphyrin, J. Phys. Chem. C 121 (2017) 4816–4824. 10.1021/acs.jpcc.6b11251.
- [23] M. A. Gordillo, D. K. Panda, S. Saha, Efficient MOF-Sensitized Solar Cells Featuring Solvothermally Grown [100]-Oriented Pillared Porphyrin Framework-11 Films on ZnO-FTO Surfaces, ACS Appl. Mater. Interfaces 11 (2019) 3196–3206. <a href="https://doi.org/10.1021/acsami.8b17807">10.1021/acsami.8b17807</a>.
- [24] M. G. Campbell, D. Sheberla, S. F. Liu, T. M. Swager, M. Dincă, Cu<sub>3</sub>(Hexaiminotriphenylene)<sub>2</sub>: An Electrically Conductive 2D Metal-Organic Framework for Chemiresistive Sensing. Angew. Chem. Int. Ed. 54 (2015) 4349–4352. 10.1002/anie.201411854.
- [25] M. G. Campbell, S. F. Liu, T. M. Swager, M. Dincă, Chemiresistive Sensor Arrays from Conductive 2D Metal-Organic Frameworks. J. Am. Chem. Soc. 137 (2015) 13780–13783. 10.1021/jacs.5b09600.
- [26] M.-S. Yao, X.-J. Lv, Z.-H. Fu, W.-H. Li, W.-H. Deng, G.-D. Wu, G. Xu, Layer-by-Layer Assembled Conductive Metal-Organic Framework Nanofilms for Room-Temperature Chemiresistive Sensing. Angew. Chem. Int. Ed. 56 (2017) 16510–16514. 10.1002/anie.201709558.
- [27] V. Rubio-Gimenez, N. Almora-Barrios, G. Escorcia-Ariza, M. Galbiati, M. Sessolo, S. Tatay, C. Marti-Gastaldo, Origin of the Chemiresistive Response of Ultrathin Films of Conductive Metal-Organic Frameworks. Angew. Chem. Int. Ed. 57 (2018) 15086–15090. 10.1002/anie.201808242.
- [28] M. L. Aubrey, M. T. Kapelewski, J. F. Melville, J. Oktawiec, D. Presti, L. Gagliardi, J. R. Long, Chemiresistive Detection of Gaseous Hydrocarbons and Interrogation of Charge Transport in Cu[Ni(2,3-Pyrazinedithiolate)<sub>2</sub>] by Gas Adsorption. J. Am. Chem. Soc. 141 (2019) 5005–5013. 10.1021/jacs.9b00654.
- [29] M.-S. Yao, J.-J. Zheng, A.-Q. Wu, G. Xu, S. S. Nagarkar, G. Zhang, M. Tsujimoto, S. Sakaki, S. Horike, K. Otake, S. Kitagawa, A Dual-Ligand Porous Coordination Polymer Chemiresistor with Modulated Conductivity and Porosity. Angew. Chem. Int. Ed. 59 (2020) 172–176. 10.1002/anie.201909096.
- [30] W.-T. Koo, J.-S. Jang, I.-D. Kim, Metal-Organic Frameworks for Chemiresistive Sensors. Chem 5 (2019) 1938–1963. 10.1016/j.chempr.2019.04.013.
- [31] E. M. Miner, T. Fukushima, D. Sheberla, L. Sun, Y. Surendranath, M. Dincă, Electrochemical Oxygen Reduction Catalysed by Ni<sub>3</sub>(Hexaiminotriphenylene)<sub>2</sub>, Nat. Commun. 7 (2016) 10942. https://doi: 10.1038/ncomms10942.
- [32] E. M. Miner, L. Wang, M. Dincă, Modular O<sub>2</sub> Electroreduction Activity in Triphenylene-Based Metal-Organic Frameworks, Chem. Sci. 9 (2018) 6286–6291. <u>10.1039/C8SC02049C</u>.

- [33] S. Lin, Y. Pineda-Galvan, W. A. Maza, C. C. Epley, J. Zhu, M. C. Kessinger, Y. Pushkar, A. J. Morris, Electrochemical Water Oxidation by a Catalyst-Modified Metal-Organic Framework Thin Film, ChemSusChem 10 (2017) 514–522. 10.1002/cssc.201601181.
- [34] C. A. Downes, S. C. Marinescu, Electrocatalytic Metal—Organic Frameworks for Energy Applications, ChemSusChem 10 (2017) 4374–4392. <a href="https://doi.org/10.1002/cssc.201701420">10.1002/cssc.201701420</a>.
- [35] F. Gándara, F. J. Uribe-Romo, D. K. Britt, H. Furukawa, L. Lei, R. Cheng, X. Duan, M. O'Keeffe, O. M. Yaghi, Porous, Conductive Metal-Triazolates and Their Structural Elucidation by the Charge-Flipping Method, Chem. Eur. J. 18 (2012) 10595–10601. 10.1002/chem.201103433.
- [36] L. Sun, T. Miyakai, S. Seki, M. Dincă, Mn₂(2,5-Disulfhydrylbenzene-1,4-Dicarboxylate): A Microporous Metal–Organic Framework with Infinite (-Mn-S-)<sub>∞</sub> Chains and High Intrinsic Charge Mobility, J. Am. Chem. Soc. 135 (2013) 8185–8188. 10.1021/ja4037516.
- [37] L. Sun, C. H. Hendon, M. A. Minier, A. Walsh, M. Dincă, Million-Fold Electrical Conductivity Enhancement in Fe<sub>2</sub>(DEBDC) versus Mn<sub>2</sub>(DEBDC) (E = S, O), J. Am. Chem. Soc. 137 (2015) 6164–6167. 10.1021/jacs.5b02897.
- [38] L. Sun, C. H. Hendon, S. S. Park, Y. Tulchinsky, R. Wan, F. Wang, A. Walsh, M. Dincă, Is Iron Unique in Promoting Electrical Conductivity in MOFs? Chem. Sci. 8 (2017) 4450–4457. 10.1039/C7SC00647K.
- [39] L. S. Xie, L. Sun, R. Wan, S. S. Park, J. A. DeGayner, C. H. Hendon, M. Dincă, Tunable Mixed-Valence Doping toward Record Electrical Conductivity in a Three-Dimensional Metal-Organic Framework. J. Am. Chem. Soc. 140 (2018) 7411–7414. 10.1021/jacs.8b03604.
- [40] M. L. Aubrey, B. M. Wiers, S. C. Andrews, T. Sakurai, S. E. Reyes-Lillo, S. M. Hamed, C.-J. Yu, L. E. Darago, J. A. Mason, J.-O. Baeg, F. Granndjean, G. J. Long, S. Seki, J. B. Neaton, P. Yang, J. R. Long, Electron Delocalization and Charge Mobility as a Function of Reduction in a Metal-Organic Framework, Nat. Mater. 17 (2018) 625–632. doi: 10.1038/s41563-018-0098-1.
- [41] J. G. Park, M. L. Aubrey, J. Oktawiec, K. Chakarawet, L. E. Darago, F. Grandjean, G. J. Long, J. R. Long, Charge Delocalization and Bulk Electronic Conductivity in the Mixed-Valence Metal—Organic Framework Fe(1,2,3-Triazolate)<sub>2</sub>(BF<sub>4</sub>)<sub>x</sub>, J. Am. Chem. Soc. 140 (2018) 8526–8534. 10.1021/jacs.8b03696.
- [42] A. Pathak, J.-W. Shen, M. Usman, L.-F. Wei, S. Mendiratta, Y.-S. Chang, B. Sainbileg, C.-M. Ngue, R.-S. Chen, M. Hayashi, T.-T. Luo, F.-R. Chen, T.W. Tseng, L.-C. Chen, K.-L. Lu, Integration of a (-Cu-S-)n Plane in a Metal-Organic Framework Affords High Electrical Conductivity, Nat. Commun. 10 (2019) 1721 (1-7). https://doi: 10.1038/s41467-019-09682-0.
- [43] T. Kambe, R. Sakamoto, K. Hoshiko, K. Takada, M. Miyachi, J.-H. Ryu, S. Sasaki, J. Kim, K. Nakazato, M. Takata, H. Nishihara, π-Conjugated Nickel Bis(Dithiolene) Complex Nanosheet, J. Am. Chem. Soc. 135 (2013) 2462–2465. 10.1021/ja312380b.
- [44] T. Kambe, R. Sakamoto, T. Kasumato, T. Pal, N. Fukui, K. Hoshiko, T. Shimojima, Z. Wang, T. Hirahara, K. Ishizaka, S. Hasegawa, F. Liu, H. Nishihara, Redox Control and High Conductivity of Nickel Bis(dithiolene) Complex π-Nanosheet: A Potential Organic Two-Dimensional Topological Insulator, J. Am. Chem. Soc. 136 (2014) 14357–14360. 10.1021/ja507619d.
- [45] J. Cui, Z. Xu, An Electroactive Porous Network from Covalent Metal–Dithiolene Links, Chem. Commun. 50 (2014) 3986–3988. 10.1039/C4CC00408F.
- [46] X. Sun, K.-H. Wu, R. Sakamoto, T. Kusamoto, H. Maeda, H. Nishihara, Conducting π-Conjugated Bis(Iminothiolato)Nickel Nanosheet, Chem. Lett. 46 (2017) 1072–1075. 10.1246/cl.170382.
- [47] A. J. Clough, J. M. Skelton, C. A. Downes, A. A. De La Rosa, J. W. Yoo, A. Walsh, B. C. Melot, S. C. Marinescu, Metallic Conductivity in a Two-Dimensional Cobalt Dithiolene Metal-Organic Framework, J. Am. Chem. Soc. 139 (2017) 10863–10867. 10.1021/jacs.7b05742.
- [48] A. J. Clough, N. M. Orchanian, J. M. Skelton, A. J. Neer, S. A. Howard, C. A. Downes, L. F. J. Piper, A. Walsh, B. C. Melot, S. C. Marinescu, Room Temperature Metallic Conductivity in a Metal-Organic Framework Induced by Oxidation, J. Am. Chem. Soc. 141 (2019) 16323–16330. 10.1021/jacs.9b06898.

- [49] R. Dong, P. Han, H. Arora, M. Ballabio, M. Karakus, Z. Zhang, C. Shekhar, P. Adler, P. S. Petkov, A. Erbe, S. C. B. Mannsfeld, C. Felser, T. Heine, M. Bonn, Z. Feng, E. Cánovas, High-Mobility Bandlike Charge Transport in a Semiconducting Two-Dimensional Metal—Organic Framework, Nat. Mater. 17 (2018) 1027–1032. 10.1038/s41563-018-0189-z.
- [50] N. Lahiri, N. Lotfizadeh, R. Tsuchikawa, V. V. Deshpande, J. Louie, Hexaaminobenzene as a building block for a Family of 2D Coordination Polymers, J. Am. Chem. Soc. 139 (2017) 19–22. 10.1021/jacs.6b09889.
- [51] J. H. Dou, L. Sun, Y. Ge, W. Li, C. H. Hendon, J. Li, S. Gul, J. Yano, E. A. Stach, M. Dincă, Signature of Metallic Behavior in the Metal-Organic Frameworks M<sub>3</sub>(Hexaiminobenzene)<sub>2</sub> (M = Ni, Cu), J. Am. Chem. Soc. 139 (2017) 13608–13611. 10.1021/jacs.7b07234.
- [52] D. Sheberla, L. Sun, M. A. Blood-Forsythe, S. Er, C. R. Wade, C. K. Brozek, A. Aspuru-Guzik, M. Dincă, High Electrical Conductivity in Ni<sub>3</sub>(2,3,6,7,10,11-Hexaiminotriphenylene)<sub>2</sub>, a Semiconducting Metal—Organic Graphene Analogue, J. Am. Chem. Soc. 136 (2014) 8859–8862. 10.1021/ja502765n.
- [53] S. Chen, J. Dai, X. C. Zeng, Metal–organic Kagome lattices  $M_3(2,3,6,7,10,11$ -hexaimino triphenylene)<sub>2</sub> (M = Ni and Cu): from semiconducting to metallic by metal substitution, Phys.Chem.Phys. 17 (2015) 5954–5958. 10.1039/C4CP05328A.
- [54] M. E. Foster, K. Sohlberg, M. D. Allendorf, A. A. Talin, Unraveling the Semiconducting/Metallic Discrepancy in Ni<sub>3</sub>(HITP)<sub>2</sub>, J. Phys. Chem. Lett. 9 (2018) 481–486. <u>10.1021/acs.jpclett.7b03140</u>.
- [55] T. Chen, J.-H. Dou, L. Yang, C. Sun, N. Libretto, G. Skorupskii, J. T. Miller, M. Dincă, Continuous Electrical Conductivity Variation in M<sub>3</sub>(Hexaiminotriphenylene)<sub>2</sub> (M = Co, Ni, Cu) MOF Alloys, *J. Am. Chem. Soc.* 142 (2020) 12367–12373. 10.1021/jacs.0c04458.
- [56] L. E. Darago, M. L. Aubrey, C. J. Yu, M. I. Gonzalez, J. R. Long, Electronic Conductivity, Ferrimagnetic Ordering, and Reductive Insertion Mediated by Organic Mixed-Valence in a Ferric Semiquinoid Metal-Organic Framework, J. Am. Chem. Soc. 137 (2015) 15703-15711. 10.1021/jacs.5b10385.
- [57] M. E. Ziebel, L. E. Darago, J. R. Long, Control of Electronic Structure and Conductivity in Two-Dimensional Metal–Semiquinoid Frameworks of Titanium, Vanadium, and Chromium, J. Am. Chem. Soc. 140 (2018) 3040–3051. 10.1021/jacs.7b13510.
- [58] M. Hmadeh, Z. Lu, Z. Liu, F. Gándara, H. Furukawa, S. Wan, V. Augustyn, R. Chang, L. Liao, F. Zhou, E. Perre, V. Ozolins, K. Suenaga, X. Duan, B. Dunn, Y. Yamamto, O. Terasaki, O. M. Yaghi, New Porous Crystals of Extended Metal-Catecholates. Chem. Mater. 24 (2012) 3511–3513. 10.1021/cm301194a.
- [59] J. A. DeGayner, I.-R. Jeon, L. Sun, M. Dincă, T. D. Harris, 2D Conductive Iron-Quinoid Magnets Ordering up to Tc = 105 K via Heterogenous Redox Chemistry, J. Am. Chem. Soc. 139 (2017) 4175–4184. 10.1021/jacs.7b00705.
- [60] L. Liu, J. A. DeGayner, L. Sun, D. Z. Zee, T. D. Harris, Reversible Redox Switching of Magnetic Order and Electrical Conductivity in a 2D Manganese Benzoquinoid Framework. Chem. Sci. 10 (2019) 4652–4661. 10.1039/C9SC00606K.
- [61] R. W. Day, D. K. Bediako, M. Rezaee, L. R. Parent, G. Skorupskii, M. Q. Arguilla, C. H. Hendon, I. Stassen, N. Gianneschi, P. Kim, M. Dincă, Single Crystals of Electrically Conductive 2D MOFs: Structural and Electrical Transport Properties, ACS Cent. Sci. 5 (2019) 1959–1964. 10.1021/acscentsci.9b01006.
- [62] D.-G. Ha, M. Rezaee, Y. Han, S. A. Siddiqui, R. W. Day, L. S. Xie, B. J. Modtland, D. A. Muller, J. Kong, P. Kim, M. Dincă, M. A. Baldo, Large Single Crystals of Two-Dimensional π-Conjugated Metal–Organic Frameworks via Biphasic Solution-Solid Growth, ACS Cent. Sci. 7 (2021) 104-109. 10.1021/acscentsci.0c01488.
- [63] J.-H. Dou, M. Q. Arguilla, Y. Luo, J. Li, W. Zhang, L. Sun, J. L. Mancuso, L. Yang, T. Chen, L. R. Parent, G. Skorupskii, N. J. Libretto, C. Sun, J. T. Miller, J. Kong, C. H. Hendon, J. Sun, M. Dincă, Atomically precise single-crystal structures of electrically conducting 2D metal–organic frameworks, Nat. Mater. 20 (2021) 222–228. <a href="https://doi.org/10.1038/s41563-020-00847-7">10.1038/s41563-020-00847-7</a>.

- [64] G. Skorupskii, M. Dincă, Electrical Conductivity in a Porous, Cubic Rare-Earth Catecholate. J. Am. Chem. Soc. 142 (2020) 6920–6924. 10.1021/jacs.0c01713.
- [65] G. Chen, L. B. Gee, W. Xu, Y. Zhu, J. S. Lezama-Pacheco, Z. Huang, Z. Li, J. T. Babicz Jr., S. Choudhury, T.-H. Chang, E. Reed, E. I. Solomon, Z. Bao, Valence-Dependent Electrical Conductivity in a 3D Tetrahydroxyquinone-Based Metal—Organic Framework, J. Am. Chem. Soc. 142 (2020) 21243–21248. 10.1021/jacs.0c09379.
- [66] C. Yang, R. Dong, M. Wang, P. St. Petkov, Z. Zhang, M. Wang, P. Han, M. Ballabio, S. A. Bräuninger, Z. Liao, J. Zhang, F. Schwotzer, E. Zschech, H. H. Klaus, E. Cánovas, S. Kaskel, T. Heine, M. Bonn, S. Zhou, T. Heine, Z. Feng, A Semiconducting Layered Metal-Organic Framework Magnet, Nat. Commun. 10 (2019) 3260. 10.1038/s41467-019-11267-w.
- [67] Y. Yue, P. Cai, X. Xu, H. Li, H. Chen, H.-C. Zhou, N. Huang, Conductive Metallophthalocyanine Framework Films with High Carrier Mobility as Efficient Chemiresistors, Angew. Chem. Int. Ed. 60 (2021)10806-10813. 10.1002/anie.202100717.
- [68] A. Yadav, D. K. Panda, S. Zhang, W. Zhou, S. Saha, Electrically Conductive 3D Metal–Organic Framework Featuring π-Acidic Hexaazatriphenylene Hexacarbonitrile Ligands with Anion–π Interaction and Efficient Charge Transport Capabilities, ACS Appl. Mater. Interfaces 12 (2020) 40613–40619. 10.1021/acsami.0c12388.
- [69] S. S. Park, E. R. Hontz, L. Sun, C. H. Hendon, A. Walsh, T. Van Voorhis, M. Dincă, Cation-Dependent Intrinsic Electrical Conductivity in Isostructural Tetrathiafulvalene-Based Microporous Metal-Organic Frameworks, J. Am. Chem. Soc. 137 (2015) 1774–1777. 10.1021/ja512437u.
- [70] L. Sun, S. S. Park, D. Sheberla, M. Dincă, Measuring and Reporting Electrical Conductivity in Metal-Organic Frameworks: Cd<sub>2</sub>(TTFTB) as a Case Study, J. Am. Chem. Soc. 138 (2016) 14772–14782. 10.1021/jacs.6b09345.
- [71] L. S. Xie, E. V. Alexandrov, G. Skorupskii, D. M. Proserpio, M. Dincă, Diverse π-π Stacking Motifs Modulate Electrical Conductivity in Tetrathiafulvalene-Based Metal-Organic Frameworks, Chem. Sci. 10 (2019) 8558-8565. 10.1039/C9SC03348C.
- [72] G. Skorupskii, B. A. Trump, T. W. Kasel, C. M. Brown, C. H. Hendon, M. Dincă, Efficient and Tunable One-Dimensional Charge Transport in Layered Lanthanide Metal-Organic Frameworks, Nat. Chem. 12 (2020) 131–136. 10.1038/s41557-019-0372-0.
- [73] J. Su, N. Xu, R. Murase, Z.-M. Yang, D. M. D'Alessandro, J.-L. Zuo, J. Zhu, Persistent Radical Tetrathiafulvalene-Based 2D Metal-Organic Frameworks and Their Application in Efficient Photothermal Conversion, Angew. Chem. Int. Ed. 60 (2021) 4789–4795. 10.1002/anie.202013811.
- [74] M. A. Gordillo, P. A. Benavides, D. K. Panda, S. Saha, Advent of Electrically Conducting Double-Helical Metal–Organic Frameworks Featuring Butterfly-Shaped Electron Rich π-Extended Tetrathiafulvalene Ligands, ACS Appl. Mater. Interfaces 12 (2020) 12955–12961. 10.1021/acsami.9b20234.
- [75] S. Zhang, D. K. Panda, A. Yadav. W. Zhou, S. Saha, Effects of intervalence charge transfer interaction between π-stacked mixed valent tetrathiafulvalene ligands on the electrical conductivity of 3D metalorganic frameworks, Chem. Sci. 12 (2021) 13379–13391. 10.1039/D1SC04338B.
- [76] Y. Kobayashi, B. Jacobs, M. D. Allendorf, J. R. Long, Conductivity, Doping, and Redox Chemistry of a Microporous Dithiolene-Based Metal—Organic Framework, Chem. Mater. 22 (2010) 4120–4122. 10.1021/cm101238m.
- [77] S. R. Ahrenholtz, C. C. Epley, A. J. Morris, Solvothermal Preparation of an Electrocatalytic Metalloporphyrin MOF Thin Film and its Redox Hopping Charge Transfer Mechanism, J. Am. Chem. Soc. 136 (2014) 2464–2472. 10.1021/ja410684q.
- [78] S. Lin, P. Usov, A. J. Morris, The Role of Redox Hopping in Metal-Organic Framework Electrocatalysis, Chem. Commun. 54 (2018) 6965–6974. 10.1039/C8CC01664J.
- [79] H. C. Wentz, G. Skorupskii, A. B. Bonfim, J. L. Mancuso, C. H. Hendon, E. H. Oriel, G. T. Sazama, M. G. Campbell, Switchable Electrical Conductivity in a Three-Dimensional Metal-Organic

- Framework via Reversible Ligand n-Doping, Chem. Sci. 11 (2020) 1342–1346. 10.1039/C9SC06150A.
- [80] M. A. Gordillo, P. A. Benavides, K. Spalding, S. Saha, A New Electrically Conducting Sinusoidal Metal-Organic Framework Featuring U-Shaped *cis*-Dipyridyl Tetrathiafulvalene Ligands, Front. Chem. 2021, 10.3389/fchem.2021.726544.
- [81] S. Goswami, I. Hod, J. D. Duan, C.-W. Kung, M. Rimoldi, C. D. Malliakas, R. H. Palmer, O. K. Farha, J. T. Hupp, Anisotropic Redox Conductivity within a Metal–Organic Framework, J. Am. Chem. Soc. 141 (2019) 17696–17702. 10.1021/jacs.9b07658.
- [82] A. M. Ullman, J. W. Brown, M. E. Foster, F. Léonard, K. Leong, V. Stavila, M. D. Allendorf, Transforming MOFs for Energy Applications Using Guest@MOF Concept, Inorg. Chem. 55 (2016) 7233–7249. 10.1021/acs.inorgchem.6b00909.
- [83] M. D. Allendorf, R. Medishetty, R. A. Fischer, Guest Molecule as a Design Element for Metal-Organic Frameworks, MRS Bull. 41 (2016) 865–869. 10.1557/mrs.2016.244.
- [84] M. D. Allendorf, M. E. Foster, F. Léonard, V. Stavila, P. L. Feng, F. P. Doty, K. Leong, E. Y. Ma, S. R. Johnston, A. A. Talin, Guest-Induced Emergent Properties in Metal–Organic Frameworks, J. Phys. Chem. Lett. 6 (2015) 1182–1195. 10.1021/jz5026883.
- [85] A. A. Talin, A. Centrone, A. C. Ford, M. E. Foster, V. Stavila, P. Haney, R. A. Kinney, V. Szalai, F. E. Gabaly, H. P. Yoon, F. Léonard, M. D. Allendorf, Tunable Electrical Conductivity in Metal-Organic Framework Thin-Film Devices, Science 343 (2014) 66–69. doi:10.1126/science.1246738.
- [86] Z. Guo, D. K. Panda, M. A. Gordillo, A. Khatun, H. Wu, W. Zhou, S. Saha, Lowering Band Gap of an Electroactive Metal–Organic Framework via Complementary Guest Intercalation, ACS Appl. Mater. Interfaces 9 (2017) 32413–32417. <a href="https://doi.org/10.1021/acsami.7b07292">10.1021/acsami.7b07292</a>.
- [87] Z. Guo, D. K. Panda, K. Maity, D. Lindsey, T. G. Parker, T. E. Albrecht-Schmitt, J. L. Barreda-Esparza, P. Xiong, W. Zhou, S. Saha, Modulating electrical conductivity of metal–organic framework films with intercalated guest π-systems, J. Mater. Chem. C 4 (2016) 894–899. 10.1039/C5TC02232K.
- [88] C.-W. Kung, K. Otake, C. T. Buru, S. Goswami, Y. Cui, J. T. Hupp, A. M. Spokoyny, O. K. Farha, Increased Electrical Conductivity in a Mesoporous Metal–Organic Framework Featuring Metallacarboranes Guests, J. Am. Chem. Soc. 140 (2018) 3871–3875. 10.1021/jacs.8b00605.
- [89] B. Le Ouay, M. Boudot, T. Kitao, T. Yanagida, S. Kitagawa, T. Uemura, Nanostructuration of PEDOT in Porous Coordination Polymers for Tunable Porosity and Conductivity, J. Am. Chem. Soc. 138 (2016) 10088–10091. 10.1021/jacs.6b05552.
- [90] M. W. A. MacLean, T. Kiato, T. Suga, M. Mizuno, S. Seki, T. Uemura, S. Kitagawa, Unraveling Interand Intrachain Electronics in Polythiophene Assemblies Mediated by Coordination Nanospaces. Angew. Chem. Int. Ed. 55 (2016) 708–713. 10.1002/anie.201510084.
- [91] B. Dhara, S. S. Nagarkar, J. Kumar, V. Kumar, P. K. Jha, S. K. Ghosh, S. Nair, N. Ballav, Increase in Electrical Conductivity of MOF to Billion-Fold upon Filling the Nanochannels with Conducting Polymer, J. Phys. Chem. Lett. 7 (2016) 2945–2950. <a href="https://doi.org/10.1021/acs.jpclett.6b01236">10.1021/acs.jpclett.6b01236</a>.
- [92] A. Jadhav, K. Gupta, P. Ninawe, N. Ballav, Imparting Multifunctionality by Utilizing Biporosity in a Zirconium-Based Metal-Organic Framework, Angew. Chem. Int. Ed. 132 (2020) 2235– 2239. 10.1002/anie.201910625.
- [93] T. C. Wang, I. Hod, C. O. Audu, N. A. Vermeulen, S. T. Nguyen, O. K. Farha, J. T. Hupp, Rendering High Surface Area, Mesoporous Metal—Organic Frameworks Electronically Conductive, ACS Appl. Mater, Interfaces 9 (2017) 12584–12591. 10.1021/acsami.6b16834.
- [94] Y. Wang, L. Wang, W. Huang, T. Zhang, X. Hu, J. A. Perman, S. Ma, A metal-organic framework and conducting polymer based electrochemical sensor for high performance cadmium ions detection, J. Mater. Chem. A 5 (2017) 8385-8393. 10.1039/C7TA01066D.
- [95] R. Haldar, B. Sen, S. Hurrle, T. Kitao, R. Sankhla, B. Kühl, A. Welle, S. Heissler, G. Brenner-Weiss, P. Thissen, T. Uemura, H. Gliemann, C. Barner-Kowollik, C. Wöll, Oxidative polymerization of

- terthiophene and a substituted thiophene monomer in metal-organic framework thin films, Eur. Polymer J. 109 (2018) 162–168. 10.1016/j.eurpolymj.2018.09.040.
- [96] P. Salcedo-Abraira, A. Santiago-Portillo, P. Atienzar, P. Bordet, F. Salles, N. Guillou, E. Elkaim, H. Garcia, S. Navalon, P. Horcajada, A highly conductive nanostructured PEDOT polymer confined into the mesoporous MIL-100(Fe), Dalton Trans. 48 (2019) 9807–9817. <a href="https://doi.org/10.1039/C9DT00917E">10.1039/C9DT00917E</a>.
- [97] C. R. Wade, T. Corrales-Sanchez, T. C. Narayan, M. Dincă, Postsynthetic tuning of hydrophilicity in pyrazolate MOFs to modulate water adsorption properties, *Energy* Environ. Sci. *6* (2013) 2172–2177. 10.1039/C3EE40876K.
- [98] Q-X. Wang, C-Y. Zhang, Oriented Synthesis of One-Dimensional Polypyrrole Molecule Chains in a Metal-Organic Framework, Macromol. Rapid Commun. 32 (2011) 1610–1614. 10.1002/marc.201100305.
- [99] S. P. Armes, Optimum Reaction Condition for the polymerization of pyrrole by Iron(III) Chloride in Aqueous Solution, Synthetic Metals 20 (1987) 365–371. 10.1016/0379-6779(87)90833-2.
- [100] J. Zhang, X. S. Zhao, Conducting Polymers Directly Coated on Reduced Graphene Oxide Sheets as High-Performance Supercapacitor Electrodes, J. Phys. Chem. C 116 (2012) 5420–5426. 10.1021/jp211474e.
- [101] G. Ćirić-Marjanović, S. Mentus, I. Pašti, N. Gavrilov, J. Krstić, J. Travas-Sejdic, L. T. Strover, J. Kopecká, Z. Moravková, M. Trchová, J. Stejskal, Synthesis, Characterization, and Electrochemistry of Nanotubular Polypyrrole and Polypyrrole-Derived Carbon Nanotubes, J. Phys. Chem. C 118 (2014) 14770–14784. 10.1021/jp502862d.
- [102] J. D. Yi, R. Xi, Z. L. Xie, G. L. Chai, T. F. Lu, R. P. Chen, Y. B. Huang, R. Cao, Highly Selective CO <sub>2</sub> Electroreduction to CH <sub>4</sub> by In Situ Generated Cu <sub>2</sub> O Single-Type Sites on a Conductive MOF: Stabilizing Key Intermediates with Hydrogen Bonding, Angew. Chem. Int. Ed. 59 (2020) 23641–23648. 10.1002/anie.202010601
- [103] J. D. Yi, D. H. Shi, R. Xie, Q. Yin, M. D. Zhang, Q. Wu, G. L. Chai, Y. B. Huang, R. Cao, Conductive Two-Dimensional Phthalocyanine-based Metal–Organic Framework Nanosheets for Efficient Electroreduction of CO<sub>2</sub>, Angew. Chem. Int. Ed. 60 (2021) 17108–17114. 10.1002/anie.202104564
- [104] D. L. Meng, M. D. Zhang, D. H. Shi, M. J. Mao, Y. Hou, Y. B. Huang, R. Cao, Highly Selective Tandem Electroreduction of CO<sub>2</sub> to Ethylene over Atomically Isolated Nickel–Nitrogen Site/Copper Nanoparticle Catalysts, Angew. Chem. Int. Ed. 60 (2021) 25485–25492. 10.1002/anie.202111136
- [105] Q. Wu, R. K. Xie, M. J. Mao, G. L. Chai, J. D. Yi, S. S. Zhao, Y. B. Huang, R. Cao, Integration of Strong Electron Transporter Tetrathiafulvalene into Metalloporphyrin-Based Covalent Organic Framework for Highly Efficient Electroreduction of CO<sub>2</sub>, ACS Energy Lett. 5 (2020) 1005–1012. 10.1021/acsenergylett.9b02756